Magnetic structure of Fe/Gd multilayers determined by resonant x-ray magnetic scattering

N. Ishimatsu* and H. Hashizume[†]

Materials and Structure Laboratory, Tokyo Institute of Technology, Nagatsuta, Midori, Yokohama 226-8503, Japan

S. Hamada and N. Hosoito

Institute for Chemical Research, Kyoto University, Uji 611-0011, Japan

C. S. Nelson,[‡] C. T. Venkataraman, G. Srajer, and J. C. Lang

Advanced Photon Source, Argonne National Laboratory, Argonne, Illinois 60439

The magnetic structures of a $(Fe/Gd)_{15}$ multilayer are determined by resonant x-ray magnetic scattering using circular polarized light of energies tuned close to the Gd L and the Fe K absorption edges. Difference superlattice Bragg peaks observed by flipping the photon helicity show that the magnetic moments of the Gd layers are directed antiparallel to the in-plane applied field at temperatures higher than 180 K, and are twisted below. The local Gd magnetizations in each 5.4-nm-thick layer are highly nonuniform in both magnitude and twist angle in the out-of-plane direction: the interface sublayers nearly fully magnetize at room and low temperatures under the influence of the adjacent Fe magnetizations, whereas the central sublayers show measurable spontaneous magnetizations at 200 K and below. An application of the $1-(T/T_c)$ law shows a reduced Curie temperature ($T_c=214$ K) compared with bulk Gd for the central sublayers, while $T_c=1023$ K for the interface sublayers. The interface and central sublayers exhibit distinct twist behaviors as a function of temperature below the compensation temperature, indicating the short-range nature of the Fe-Gd interaction. The element-specific resonant x-ray scattering confirmed the antiferromagnetic arrangement of the Gd and Fe moments at room temperature. [S0163-1829(99)03037-4]

I. INTRODUCTION

Fe/Gd multilayers with alternately stacked iron and gadolinium layers show a reversible change of magnetic structure between the aligned and twisted states depending on the strength H of an applied in-plane field and on temperature T.[1–7] The antiferromagnetically coupled Fe and Gd moments line up with the applied field in the aligned state, whereas they make finite in-plane angles to the field in the twisted state. At a fixed H, the state change occurs near the compensation temperature, where the iron and gadolinium layers have similar magnetizations of opposite signs, thereby yielding a minimal net magnetization in the multilayer. In this temperature regime, the multilayer in a low external magnetic field tends to decrease the sum of the Zeeman energy and the exchange energy by arranging the Fe and Gd moments noncollinear with the applied field like in spin-flopped antiferromagnets. Theoretical modeling of the aligned-to-twisted phase transition shows that the decrease in the Zeeman energy by directing the antiparallel Gd (Fe) moments towards the parallel orientation is larger than the sum of the increase in the Zeeman energy by directing the parallel Fe (Gd) moments away from the field direction and the increase in the exchange energy by destroying the antiferromagnetic configuration of the Fe and Gd moments.[1,2]

Our previous resonant x-ray magnetic scattering experiment confirmed the presence of canted Gd moments in the twisted state of an Fe/Gd multilayer.[8] The difference signal, I^+-I^-, observed at the Gd L edge, showed finite multilayer Bragg peaks in the $\phi=90°$ geometry in which the plane of x-ray scattering made a 90° angle to the applied field. The

difference Bragg peaks observed in the $\phi=0°$ and 90° geometries showed $-$ and $+$ signs, i.e., negative and positive profiles, in the odd- and even-order reflections, for both aligned and twisted states. It was suggested that this feature originates from nonuniform magnetizations of gadolinium layers over the 5-nm thickness.[8]

Resonant x-ray magnetic scattering has proven to be a useful technique to study magnetism. It profits from the significant enhancement of the magnetic scattering signal when the x-ray photon energy is tuned to an absorption edge.[9–11] The resonant enhancement is particularly pronounced at the spin-orbit split L and M edges of the $3d$, $4f$, and $5f$ magnetic atoms. The availability of intense, energy-tunable, highly polarized x rays from synchrotron sources has enabled resonant x-ray magnetic scattering to become a powerful probe of magnetic structures in surfaces[12,13] and thin films.[8,14–21] The signal is element specific and can be as large as several percent of Thomson scattering, in contrast to the nonresonant magnetic scattering that is not element specific and is typically three orders of magnitude weaker in amplitude than Thomson scattering. At small scattering angles 2θ a circular polarized probing beam is required because of the $\tan 2\theta$ factor involved in the scattering of plane polarized x rays.[15] The observed signal includes pure charge scattering, pure magnetic scattering (resonant and nonresonant components) and charge-magnetic interference scattering.[22] The last component is isolated by calculating a difference, I^+-I^-, of the two scattering intensities measured with right-handed (+ helicity) and left-handed (− helicity) circular polarized probing photons. The helicity flip technique is preferable to field reversal, as all magnetic moments in a
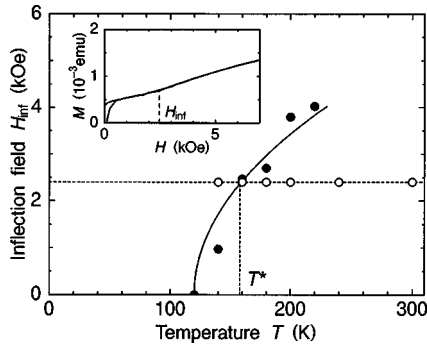
FIG. 1. Inflection fields H_{inf} versus temperature T (closed circles) for the magnetization curves observed from the Fe/Gd multilayer. The solid line is a guide to eye. Open circles show the temperatures at which the magnetic x-ray scattering data were collected. The inset shows a typical magnetization curve.

nonsaturated magnet do not necessarily reverse their directions in a reversed external field. The interference signal is only sensitive to the magnetization component parallel to the plane of scattering. This allows us to study the spatial orientations of local magnetic moments in ferromagnets. The technique features a high momentum resolution and surface sensitivity. A much smaller sample volume is required than in neutron scattering.

In this paper, we first describe in Sec. II an experiment which measured the resonant magnetic specular reflections from a $[\text{Fe(3.5nm)/Gd(5.4nm)}]_{15}$ multilayer using a circular polarized probing beam. Our previous Fe/Gd sample, for which x-ray data were presented elsewhere,[8] had no protective surface layer and could have been affected by oxidation. We prepared a new sample and repeated x-ray measurements for the present work. In Sec. III, we determine the magnitudes and orientations of local magnetizations in the aligned and twisted states of our sample, using the newly developed formulas which are presented in the Appendix. In Sec. IV, we discuss the derived structures by comparing them with data from other experiments. Finally, Sec. V concludes the paper.

II. EXPERIMENT

A. Procedure

The Fe/Gd multilayer investigated has 15 bilayers of 3.5-nm-thick Fe and 5.2-nm-thick Gd (design values), grown on a silicon (111) wafer in a vacuum-deposition chamber (3 $\times 10^{-7}$ Pa) equipped with E-gun evaporators and a quartz thickness monitor. The substrate was kept at room temperature, and the first grown layer was Gd and the last layer was Fe. The deposition rate was 1.2–1.8 nm/min for both Fe and Gd. A protective silicon layer, 3.5 nm in thickness, was deposited on the top surface. X-ray diffraction scans showed that both iron and gadolinium layers are polycrystalline. An identical multilayer was grown on a Kapton film in the same deposition run for magnetization measurements. The magnetization ($M-H$) curves, measured at various temperatures using a SQUID magnetometer with a field applied parallel to the sample surface, showed rapid initial increases. This was followed by a slower rise in which an inflection was observed (inset in Fig. 1) for temperatures (T) between 240 and

140 K, indicative of field-induced magnetic structure changes in the multilayer. Figure 1 is a plot of the inflection fields H_{inf} versus T. We expect that the sample is in an aligned state on the right of the traced curve and in a twisted state on the left.[2] At a fixed field, $H = 2.4\,\text{kOe}$, for example, the transition should occur at T^* close to 160 K.

We collected magnetic x-ray data on the SRI-CAT (Synchrotron Radiation Instrumentation Collaborative Access Team) 1-ID beamline at the Advanced Photon Source, Argonne National Laboratory, using circular polarized x-ray beams of energies tuned close to the L_3 absorption edge of Gd. The setup and the measurement procedure are similar to those reported previously.[8] We controlled the undulator gap distance in the light source to maximize the photon flux at 7.25 keV in the first harmonic peak. The beamline optics used a cryogenically cooled Si(111) double-crystal monochromator, followed by a diamond quarter-wavelength plate and a flat harmonics-rejection mirror. The phase plate, 0.4 mm in thickness, was in the symmetric Bragg-case 111 reflection, and the transmitted beam was used for the experiment. The Fe/Gd sample, $4 \times 4 \times 0.6\,\text{mm}$ in size, was mounted inside a Displex cryostat with a NdFeB magnet. Purpose built pole pieces allowed an in-plane field (H) to be applied to the sample without blocking the grazing x-ray beams in arbitrary azimuthal directions. All data were collected with $H = 2.4\,\text{kOe}$. We flipped the photon helicity by oscillating the diamond plate, with a piezoelectric actuator, between the $+0.42$ and -0.42 mrad positions offset from the 111 Bragg peak during $\theta - 2\theta$ scans, which measured specular reflections from the sample at room and low temperatures. The sum intensity $I^+ + I^-$ represents the charge scattering, while the difference $I^+ - I^-$ is due to the resonant magnetic-charge interference scattering.[19] A dynamical-theory calculation indicated $-$ $(+)$ helicity for the $+$ $(-)$ offset position of the diamond in the setup used. The estimated degree of circular polarization in the transmitted x-ray beam is 0.994. The whole cryostat was rotated by 90° on the ϕ axis of a Huber goniometer to switch the $\phi=0°$ and 90° geometries.

Prior to the scattering experiment, we located the photon energies (E) at which resonant enhancement occurs on the magnetic circular dichroic (MCD) absorption spectrum of a metal Gd foil. The bulk of our Fe/Gd scattering data was collected using photons of 7243.5 eV, 2 eV below the MCD peak observed at the Gd L_3 edge. The MCD data also served to evaluate the resonant magnetic scattering factors of Gd atoms (Fig. 2). The real part $f'_m(\text{Gd})$ was derived from the measured imaginary part $f''_m(\text{Gd})$ [see Eq. (2)] using the Kramers-Kronig relation.

In all plots to be presented hereafter, $I^+(I^-)$ is the signal measured with a $+$ $(-)$ field applied on the sample. We define the direction of an in-plane field with reference to the helicity vector of the incoming x-ray beam as shown in Fig. 3 which is taken from Ref. 8. In the $\phi=0°$ geometry, the field is $+$ $(-)$ when the **B** vector is directed parallel (antiparallel) to the projected helicity vector. Circular polarized light with $+$ $(-)$ helicity has a helicity vector parallel (antiparallel) to the wave vector **k**. The field directed towards the downstream x ray is then $+$ $(-)$ for light with $+$ $(-)$ helicity in our definition. In the $\phi=90°$ geometry, the **B** vector of the $+$ $(-)$ field is rotated clockwise (counterclockwise) from
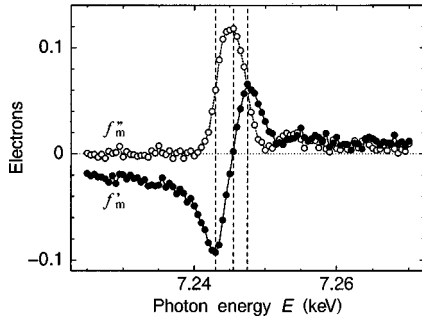
FIG. 2. Resonant magnetic scattering factors of Gd atoms near the L_3 absorption edge versus photon energy E. f'_m: real part, f''_m: imaginary part. Error bars are smaller than the size of the symbols. The broken vertical lines show the three photon energies used to take the data shown in Fig. 6.

the projected helicity vector, as viewed with the scattering vector **q** head on. In our definition, $I^+(I^-)$ is the x-ray intensity measured with a field of a same (opposite) sign as the photon helicity of the incoming beam. One can use an alternative definition for field direction, but an unambiguous definition is essential to unique determination of the magnetization orientation from x-ray data.

B. Results

Figure 4 plots the average intensities $(I^+ + I^-)/2$ measured from the Fe/Gd sample at $E = 7243.5$ eV and $T \sim 300$ K in the $\phi = 0°$ geometry. The prominent four Bragg peaks indicate a highly ordered chemical structure of the multilayer. The reflectivity profile is consistent with the layer-thickness $t_{Fe} = 3.48 \pm 0.11$ and $t_{Gd} = 5.43 \pm 0.11$ nm, determined by a fit of a similar profile recorded on a laboratory reflectometer at a $CuK\alpha$ x-ray source. The least-squares fit refined the uniform electron densities in the iron and gadolinium layers to 0.88 ± 0.05 and 0.97 ± 0.06 relative to those of bulk bcc Fe and hcp Gd, respectively. A value of 0.81 ± 0.06 nm was obtained for the root-mean-square roughness at the Fe/Gd interfaces. We evaluated the chemical structure parameters at the off-edge energy, where the anomalous dispersion effects are unimportant and the scattering factors are more accurately known.

Figure 5(A) shows $(I^+ - I^-)/(I^+ + I^-)_{Bragg}$ for the four Bragg peaks, observed in the $\phi = 0°$ and $90°$ geometries for $T = 300$, 240, 200, 180, 160, and 140 K. The ordinate shows the x-ray counts of the difference intensities divided by those of the sum intensities at the individual Bragg peaks. A salient feature in Fig. 5(A) is the reversed signs of the odd- and even-order Bragg peaks. The first-order peaks are obscured by the photon statistics but appear to have negative profiles accompanied by positive bumps or plateaus on the low 2θ flanks at some temperatures. In Fig. 5(A) for $\phi = 90°$, definite peaks are observed at 160 and 140 K, whereas peaks are much less prominent at and above 180 K. This indicates finite perpendicular components of the Gd magnetic moments in the sample at 160 and 140 K, which vanish at and above 180 K. Taken together with the finite peaks at all temperatures in Fig. 5(A) for $\phi = 0°$, the result shows that the Gd moments are aligned with the external field above a temperature between 160 and 180 K and are canted below. This picture is consistent with the H_{inf} behavior in Fig. 1.
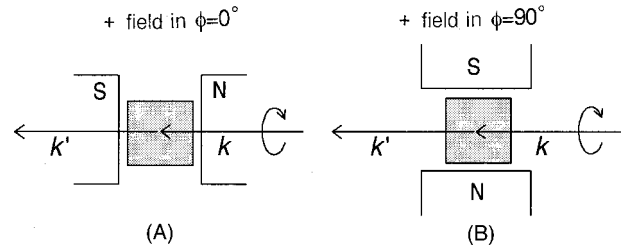
FIG. 3. The $\phi = 0°$ (A) and $\phi = 90°$ (B) geometries. The **B** vector of the applied magnetic field is parallel (A) and perpendicular (B) to the plane of scattering defined by **k** and **k**′. The scattering vector **q** is pointing out of the page. For a right circular polarized probing beam (**k**), the field direction is positive in both (A) and (B) by the convention described in the text.

Figure 6(A) compares the normalized difference specular peaks observed with photons of slightly shifted energies, $E = 7243.0$, 7245.5, and 7247.5 eV, at $T \sim 300$ K and $\phi = 0°$. There is a clear sign-change in the Bragg peaks at 7247.5 eV. This is due to the energy variations of the scattering factors of Gd atoms near the L_3 edge. At the three energies chosen, the real part of the resonant magnetic scattering factor, $f'_m(Gd)$, is negatively maximal, nearly zero, and positively maximal (Fig. 2). Figure 6(A) shows a strong E dependence of the resonant x-ray magnetic scattering, although the profile change observed is not solely due to the varied $f'_m(Gd)$ and $f''_m(Gd)$. The resonant magnetic-charge interference scattering is affected by the E-dependent charge scattering factors $f'_c(Gd)$ and $f''_c(Gd)$, as well, which show similar strength variations to the magnetic scattering factors in the vicinity of the absorption edge.[23]

In all data presented thus far, Gd is in resonance, but the preliminary data in Fig. 7(A) were obtained at $E = 7111.0$ eV close to the Fe K absorption edge ($T \sim 300$ K, $\phi = 0°$). All difference Bragg peaks show positive profiles. The chosen x-ray energy is located 0.5 eV above the negative peak in an MCD spectrum measured with an iron foil, where $f''_m(Fe) > 0$. A K-K conversion showed a positive $f'_m(Fe)$ at this energy.

III. MAGNETIC STRUCTURE MODELS

Using Eq. (A11), a number of models were tested to simulate the observed difference Bragg peak profiles, showing the $-$, $+$, $-$, and $+$ signs for the first-, second-, third-,
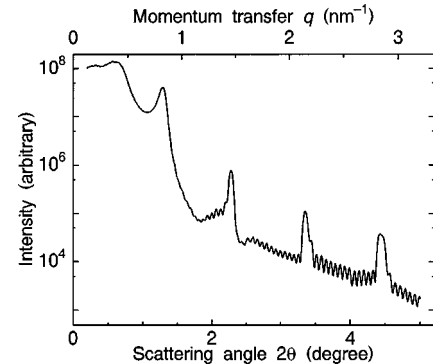
FIG. 4. Charge specular reflection profile of the Fe/Gd multilayer sample measured at the Gd L_3 edge.
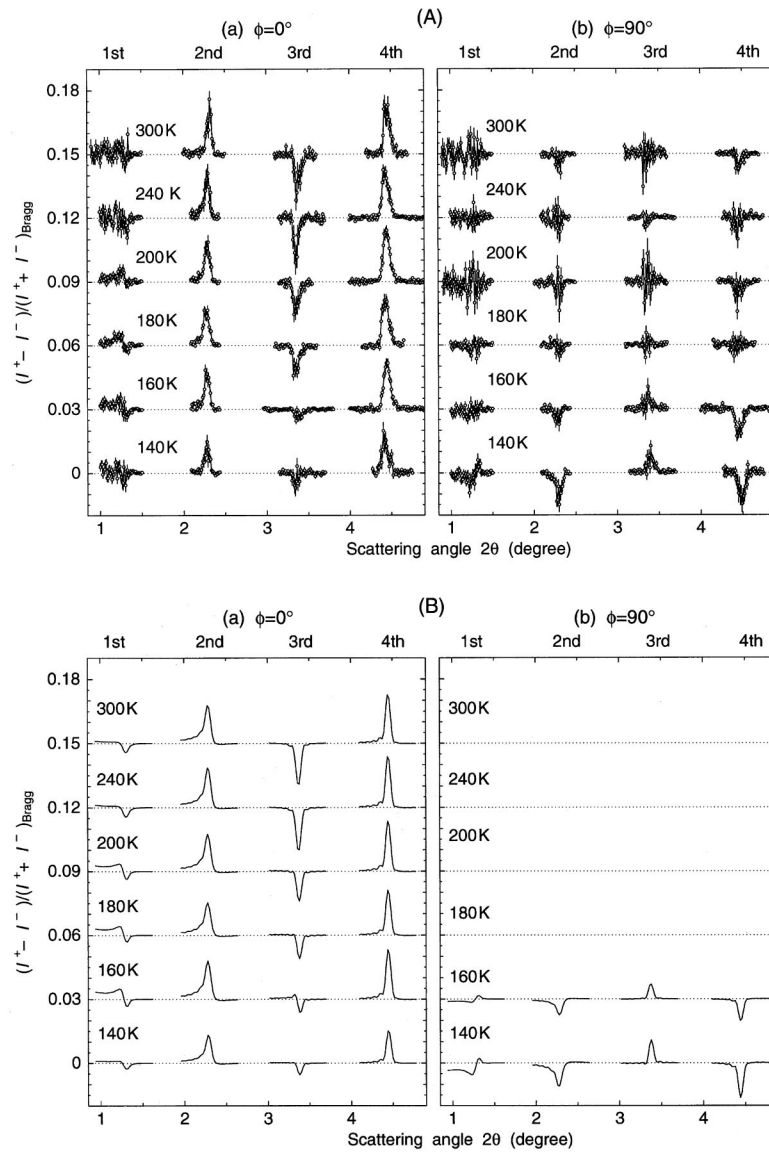
FIG. 5. Temperature variation of the first-, second-, third-, and fourth-order difference Bragg peaks from the Fe/Gd multilayer sample, normalized by the x-ray counts at the individual sum Bragg peaks (not shown). (a) for the $\phi=0°$ geometry and (b) for the $\phi=90°$ geometry. (A): observed, (B): simulated. The $I^+ - I^-$ signal strengths in the $\phi=0°$ geometry at 200 K are 7196, 3689, 470, 263 cps at the first, second, third, and fourth Bragg peaks, respectively.
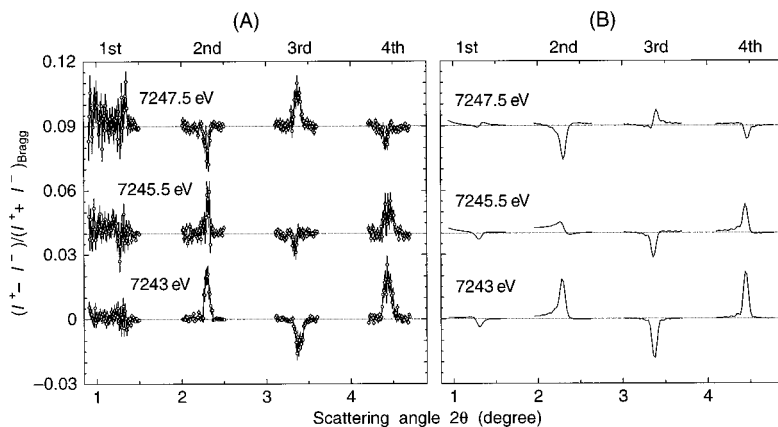
FIG. 6. Energy variation of the four normalized difference Bragg peak profiles in the vicinity of the Gd L_3 edge. (A): observed, (B): simulated.
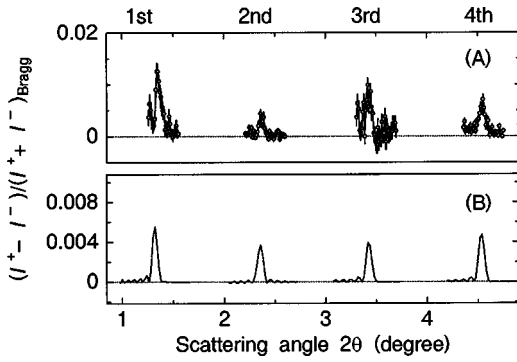
FIG. 7. Normalized difference Bragg peaks at the Fe K edge from the multilayer at room temperature. (A): observed, (B): simulated.

and fourth-order reflections, respectively, in Fig. 5(A). The resonant magnetic scattering factors of Gd atoms were read from Fig. 2 and identified as g'_m and g''_m [see Eq. (A19)]. The charge scattering factors were derived from the nonmagnetic absorption data, $I^+ + I^-$, obtained in the MCD measurement. The nonresonant Fe charge scattering factors were taken from Cromer and Liberman.[24] We assumed uniform electron densities in both iron and gadolinium layers, with abrupt changes at the interfaces. Models assuming uniform magnetizations, either positive or negative, for the fifteen gadolinium layers did not produce difference Bragg peaks of alternating signs consistent with the data. To explain the observed peaks, we had to assume that each gadolinium layer magnetized nonuniformly along the out-of-plane direction. Under the simplifying assumption that all fifteen gadolinium layers have the same magnetic structure, the observed peak sign pattern was reproduced by the models assuming larger antiparallel magnetizations in the interface regions than at the centers of the individual films. Figure 5(B) shows best fitting simulations. These are calculated from the model magnetization structures shown in Fig. 8, where each gadolinium layer is divided in twenty sublayers of equal thickness ($p=20$). The negative $S_p^{\parallel}$ in Fig. 8(A) indicates that the

parallel components of the local gadolinium magnetizations are directed opposite to the applied field. The positive $S_p^{\perp}$ in Fig. 8(B) indicates that the perpendicular components of the same magnetizations are rotated in the counterclockwise direction from the field direction when viewed from above the multilayer surface. Symmetric exponential profiles of type $a + b[\exp(-t/\tau) + \exp\{(-t_{Gd} + t)/\tau\}]$ were used to describe the nonuniform magnetization over the mean film thickness t_{Gd}, with parameters a, b, and τ varied until the main features of the data were reproduced for the individual temperatures. This function was used independently to fit the parallel and perpendicular magnetizations. For the $\phi=90°$ geometry, we assumed $a=b=0$ for temperatures higher than 180 K, where no definite Bragg peak was observed. A comparison with Fig. 5(A) shows that the calculated profiles in Fig. 5(B) well reproduce the relative Bragg-peak heights observed in the $\phi=0°$ and 90° configurations. Figure 5(B) includes no magnetic scattering from Fe. This is justified by the fact that the experimental photon energy is away from the nearest Fe absorption edge by more than 100 eV.

In Fig. 8, the gadolinium layers significantly magnetize only in the interface regions close to the iron layers at temperatures higher than 240 K. At 160 K, the twisting occurs in the interface region, but the deviation from the aligned structure is small. The twist angles of the interface magnetizations increase at 140 K, and the magnetizations in the film interior are nearly perpendicular to the field. These features are more clearly seen in Fig. 9, which shows the schematic magnetic structures composed from Fig. 8.

Further support for the derived magnetization structures is provided by the Bragg peak profiles at the shifted x-ray energies. Figure 6(B) is calculated from the $S_p^{\parallel}$ profile for 300 K, using the g'_m(Gd) and g''_m(Gd) evaluated in Fig. 2 at the relevant energies. The Bragg peaks of reversed signs for $E=7247.5$ eV are nicely reproduced. A closer comparison with Fig. 6(A) shows a fairly good agreement in the relative peak heights.

Because of the antiferromagnetic coupling of Fe with Gd at the layer interfaces, the iron moment may be directed par-
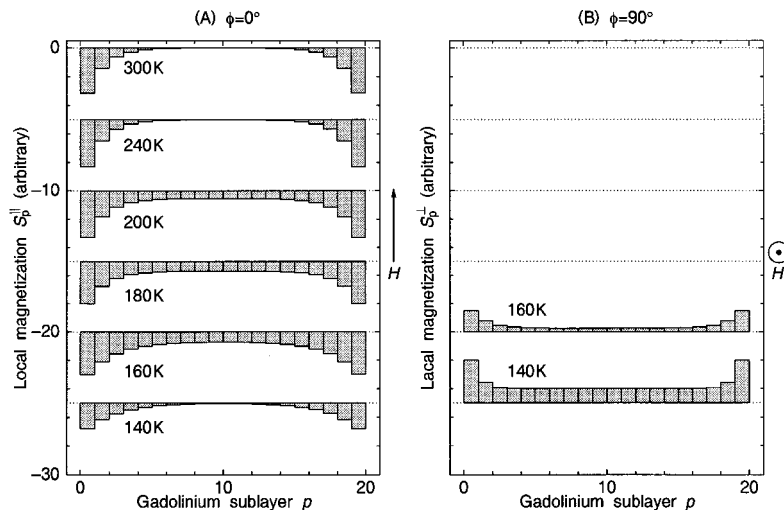
FIG. 8. Model magnetization structures for the gadolinium layer. A 5.43-nm-thick gadolinium layer is divided into twenty sublayers to calculate the difference Bragg peak profiles shown in Fig. 5(B). (A) for the $\phi=0°$ geometry and (B) for the $\phi=90°$ geometry. The applied field H is directed upward in (A) and out of the page in (B).
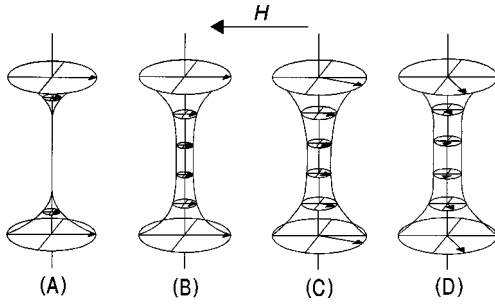
FIG. 9. Schematic magnetization structures of the gadolinium layer in the Fe/Gd multilayer for 300 K (A), 200 K (B), 160 K (C), and 140 K (D). Arrows show the strengths and directions of local Gd magnetizations over a 5.43-nm-thick gadolinium layer. H indicates the applied in-plane field direction. The multilayer surface is located towards the top of the diagrams.

FIG. 10. Comparison of the measured multilayer magnetizations (closed circles and solid line) with those estimated from the structure models shown in Fig. 8 (open circles).

allel to the applied field at temperatures higher than 180 K, where the gadolinium moments are found antiparallel (Fig. 9). This is evidenced in Fig. 7(B), calculated for a parallel, uniform magnetization in the fifteen iron layers. The result confirms that our Fe/Gd multilayer is in the Fe-aligned state at room temperature.[2,7]

IV. DISCUSSION

Figures 8 and 9 uniquely specify the orientations of local gadolinium magnetizations in our Fe/Gd multilayer with respect to the direction of the applied in-plane field. The result critically depends on the signs assigned to the various quantities in the chain of x-ray experiment and data handling. A wrong sign assignment could lead to totally different structures. There have been disputes about the sign of the MCD signal at the Gd L_3 edge. According to our field sign convention, we define the MCD absorption coefficient μ_m by

$$\mu_m t = \mu^+ t - \mu^- t = -\ln(I^+/I_0) + \ln(I^-/I_0), \quad (1)$$

where $\mu^+ (\mu^-)$ is the absorption coefficient measured with an applied magnetic field of the same (opposite) sign as the photon helicity. The MCD spectrum we observed shows a simple negative peak at the Gd L_3 edge, indicating $\mu_m < 0$. This is consistent with Baudelet et al.[25] who observed a positive peak but defined μ_m by $\mu^- - \mu^+$. The imaginary part of the resonant magnetic scattering factor f_m'' is related to μ_m via

$$\mu_m = -(8\pi n_0 r_e/k)(\hat{\mathbf{k}} \cdot \hat{\mathbf{z}}) f_m'', \quad (2)$$

where $\hat{\mathbf{k}} \cdot \hat{\mathbf{z}}$ is the direction cosine of the Gd moment with respect to the incident x-ray wave vector. We determined $f_m''(Gd)$ from the experimental μ_m assuming that all Gd atoms in the metal Gd foil at 200 K have magnetic moments parallel to the applied field. This assumption affects the sign and magnitude of the obtained $f_m''(Gd)$, and hence those of the real part $f_m'(Gd)$, shown in Fig. 2. Our $f_m'(Gd)$ and $f_m''(Gd)$ values involve errors no smaller than 10%. A major error source is the offset level defined in the $\ln I^+ - \ln I^-$ data to evaluate μ_m. We removed a reproducible offset I_b from I^+ to bring $\ln(I^+ - I_b) - \ln I^-$ to the zero level at off-edge energies, but this process could introduce an error of several
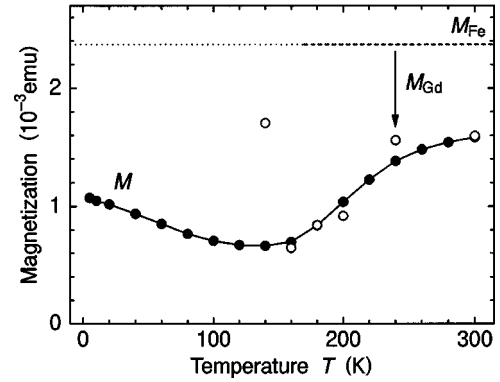
percent in the $f_m''(Gd)$ values. The origin of I_b is not clear. Nonequal intensities of the $+$ and $-$ beams on the Gd foil are not responsible because the measurement was made for a fixed count on the monitor ion chamber placed after the diamond phase plate. An additional error of several percent could result from the error in the foil thickness (t) measurement. These errors affect g_m' and g_m'' in Eq. (A19), but not S_p. Hence the structure model in Fig. 8 is independent of the scattering factor errors.

We measured I^+ and I^- using the x-ray beams transmitted through the diamond plate set at $+0.42$ and -0.42 mrad off the Bragg position. One may wonder if this ensures the same momentum transfer $\mathbf{q}$ in the specular reflection measurements on the multilayer. Dynamical diffraction theory guarantees that the transmitted beam through a plane-parallel crystal is parallel to the primary incoming beam at an arbitrary angular setting of the crystal.

Our chemical model of the multilayer, assuming equal, uniform electron densities in the individual layers with sharp interfaces, appears to be too simple in view of Lee et al.[20] who report significantly graded Fe/Gd interfaces in their multilayer. However, our model appears to be a reasonable approximation because it fits well the measured nonmagnetic specular reflectivity profile over a large q_z range of 0.1 ~ 4.5 nm^{-1} for the Cu$K\alpha$ radiation. Agreement of the calculated difference Bragg peaks with the experiment, i.e., Fig. 5(A) versus Fig. 5(B), would be improved by including roughness, chemical and magnetic,[26] at the Fe/Gd interfaces, which is all ignored in our simulations.

Figure 10 illustrates the consistency of our structure models with the magnetization measurement. The filled circles plot the magnetizations M measured at $H = 2.4$ kOe, which show a minimum near 140 K. This is close to T^* shown in Fig. 1. The open circles show the magnetizations estimated from Fig. 8(A). The net magnetization of the Fe/Gd multilayer in the Fe-aligned state may be given by $M_{Fe} - M_{Gd}$, where M_{Fe} and M_{Gd} are the total magnetizations of the fifteen iron and the fifteen gadolinium layers, respectively. The thick broken line in Fig. 10 shows M_{Fe} estimated assuming that the iron layers fully magnetize in the applied 2.4 kOe field. Using 1740 emu cm^{-3} for the saturation magnetization of bcc iron, corresponding to 2.2μ_B per Fe atom, and 3.97×10^{-6} cm^3 for the total volume (V_t) of the Fe/Gd multilayer grown on the Kapton film, estimated from the
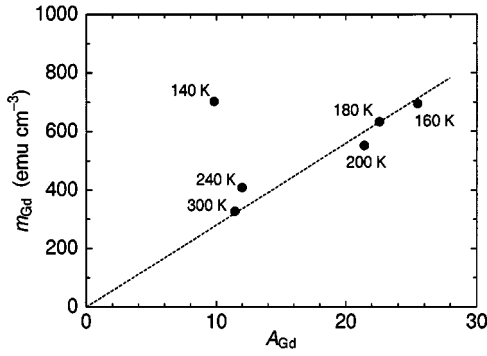
FIG. 11. Magnetizations per unit volume of the gadolinium layers estimated from the structure models shown in Fig. 8 (closed circles). Broken line shows a regression for the four high-temperature data points. See text.

FIG. 12. Hyperfine fields H_{hf} around ^{57}Fe nuclei (closed circles) determined from the Mössbauer experiment at room temperature. Broken line shows the hyperfine field expected for Fe magnetic moments aligned parallel to the applied magnetic field.

known substrate area and the layer thicknesses determined from the x-ray data, the iron layers are known to contribute 2.37×10^{-3} emu to the total magnetization. This estimate includes the relative density of 0.88 for the iron layers. M_{Gd} may be given by CA_{Gd}, where A_{Gd} is the integrated area of the $S_p^{\parallel}$ histograms in Fig. 8(A) ($A_{Gd} = \Sigma_p S_p^{\parallel}$). We determined proportionality constant C as follows. Let m_{Gd} be the magnetization per unit volume of the gadolinium layer. Taking the layer thicknesses into account, we have $m_{Gd} = (1 + 3.48/5.43)(m - 598)$ emu cm^{-3}, where m is the measured magnetization per unit volume of the multilayer, $m = M/V_t$. Figure 11 is a plot of m_{Gd} versus A_{Gd}. A least-squares fit of the four data points for 300, 240, 200, and 180 K, at which the multilayer is in the aligned state, gives $m_{Gd} = 27.97 A_{Gd}$. The regression line should pass through the origin. The magnetizations $M_{Fe} - M_{Gd}$ thus estimated are in good agreement with M at 300, 240, 200, 180, and 160 K in Fig. 10. The large deviation at 140 K appears to provide another support for the twisted structure, in which the Fe moments would be canted and thus the thin broken line would be a poor estimate of M_{Fe} in the applied-field direction.

A similar process allows us to evaluate the absolute local magnetizations in the gadolinium layers. Let μ_p be the magnetization of sublayer p. Then $\Sigma_p \mu_p = 20 m_{Gd}$, and we have $\mu_p = 559.4 S_p$ emu cm^{-3}. For the interface sublayers ($p = 1$ or 20), we find $\mu_p = 1762, 1846, 1846$, and 1678 emu cm^{-3} for 300, 240, 200, and 180 K, respectively, from Fig. 8(A). These are not far from 2056 emu cm^{-3}, the saturation magnetization of bulk Gd at 0 K ($7.55 \mu_B$) corrected for the density of our gadolinium layers. It is likely that the interface sublayers nearly fully magnetize in our Fe/Gd sample. More accurate μ_p values would be obtainable by refining the chemical structure of the multilayer. Structural disorder, including varied bilayer periods, Fe/Gd interdiffusion and interface roughness, weakens the multilayer Bragg reflections, whilst not affecting the SQUID magnetization measurement.

In Fig. 9 the twisted gadolinium magnetizations are rotated counterclockwise from the external field vector **B** when viewed from above the multilayer surface. It is likely that the twist direction was determined by the transverse field of the permanent magnet. In fact, a post-experiment field measurement evidenced a small transverse field of about 100 Oe which rotated slightly the total field clockwise from the main
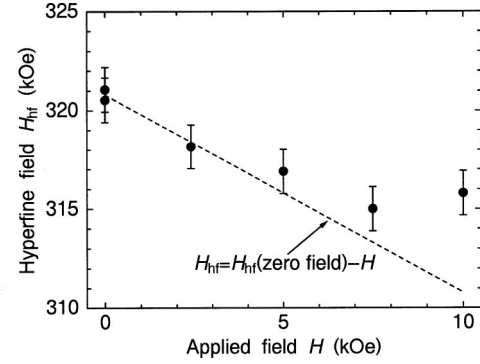
field direction. The transverse field accounts for the small Bragg peaks seen at 300, 240, 200, and 180 K in Fig. 5(A) for $\phi = 90°$. At these temperatures, the Fe magnetizations are parallel to the total field. The Gd magnetizations are thus slightly rotated counterclockwise from the main field direction. This rotation direction is maintained in the twisted state.

We conclude that Fig. 8 represents the consistent magnetization structures of the gadolinium layers. Our twist structure is similar to the so-called ''bulk twisted'' structure of Camley *et al.*[1,2] in that the average twist angle is the same in all fifteen gadolinium layers throughout the multilayer. Our result shows, however, that the local magnetization twists highly nonuniformly in each gadolinium layer along the out-of-plane direction.

To obtain support for the magnetization directions derived from the x-ray measurement, we collected Mössbauer data from a [Fe(3.5nm)/Gd(5.2nm)]$_{15}$ sample grown on a Kapton film using an ^{57}Fe-enriched iron evaporation source, at room temperature. The estimated ^{57}Fe content in the iron layers is 10%, and an x-ray specular reflectivity profile, recorded from a simultaneously grown sample on a silicon substrate, showed as high a multilayer order as in the sample used for the magnetic x-ray experiment. Filled circles in Fig. 12 show the hyperfine fields at the ^{57}Fe nuclei, H_{hf}, estimated from the spacings of the outermost resonance peaks in the Mössbauer spectra, plotted versus the in-plane field H applied to the sample. The zero-field data were measured twice, before and after the field was increased up to 10 kOe. The average H_{hf} is 320.8 ± 1.1 kOe at zero field, which decreases to 318.2 ± 1.1 at 2.5 kOe. The broken line depicts H_{hf} (zero field) $- H$, the hyperfine field expected for the Fe moments aligned parallel to the applied field. The error bars are large, but it is very likely that the Fe moments are directed parallel to the applied field at $H = 2.4$ kOe, which we used to calculate Fig. 7(B). Note that the parallel Fe moments also support the antiparallel gadolinium moments determined from the independent x-ray data but using the same technique. The increasing deviations of the Mössbauer data from the straight line at higher H in Fig. 12 do not contradict the expected field-induced aligned-to-twisted phase change of the multilayer structure and increasing rotation angles of the Fe moments away from the parallel orientation.

Clearly the large interface gadolinium magnetizations are induced by the magnetized iron layers. In Fig. 8 the film

interior does not magnetize at temperatures as low as 240 K, and shows growing spontaneous magnetizations with decreasing T below 200 K. This suggests that the Curie temperature T_c for the thin gadolinium layers is located somewhere between 240 and 200 K, which is more than 50 K lower than the T_c for bulk Gd (293 K). An application of the $2056(1-T/T_c)$ law to the interior ($p=10$) magnetizations shows $T_c=214.3$ K. The 3% smaller density in the gadolinium layers than in bulk would not explain the low T_c. It should be a thin-film effect. The same law indicates $T_c = 1023$ K for the interface sublayers ($p=1$ and 20). The elevated interface T_c, predicted by the energy calculations,[1,2] is due to the molecular field of Fe. Once the multilayer is cooled to the transition temperature T^* in the moderate external field, the interface moments appear to twist first (Fig. 9). The interior magnetizations rotate at a lower temperature but over a larger angular range than the interface magnetizations, once set in ''motion.'' This leads us to speculate that the twist of the interface magnetizations are driven and constrained by the rotating Fe moments, whereas the behavior of the interior magnetizations is dominated by the Zeeman interaction with the external field. The idea could be tested by future resonant x-ray magnetic scattering measurements at the Fe edge. Additional information would be provided by energy calculations, which are in progress.

V. CONCLUDING REMARKS

Canted magnetizations in Fe/Gd multilayers have previously been detected by Mössbauer measurements[4,6] and neutron scattering.[5,7] [57]Fe Mössbauer spectroscopy is only sensitive to Fe moments and the spin-flip neutron technique does not distinguish between the Fe and Gd. The present work gives evidence for the transition between the aligned and twisted states in the gadolinium layers. The element-specific resonant x-ray magnetic scattering has allowed us to confirm that the Fe and Gd moments in the Fe-aligned state line up parallel and antiparallel to the external field, respectively. The directions of the Fe and Gd magnetizations have been determined independently of each other. Simulation calculations using our formalism for magnetic specular reflections have enabled the local magnetizations in the 5.43-nm-thick gadolinium layers to be mapped out at a fractional nanometer resolution. The proposed structures show the strongly magnetized interface sublayers for both aligned and twisted states, indicating the short-range nature of the Fe-Gd interaction. The vanishing interior magnetizations at 240 K suggest that the thin gadolinium film has a Curie temperature much lower than bulk Gd. The twist angle of the local Gd magnetization is also nonuniform in the out-of-plane direction, indicating the influence of the adjacent Fe magnetizations on the interface twist angles. The derived magnetic structures are consistent with the magnetization measurement.

The technique of resonant x-ray magnetic scattering developed in this work is applicable to a variety of magnetic thin films and surfaces. Using the known helicity information of a circular polarized probing beam, one can determine the unique local orientations of the in-plane magnetizations of selected atom species, in addition to their strengths. Unlike Bragg reflections by crystals, the specular reflections are not restricted in x-ray wavelength nor the crystalline quality of a sample. The absorption edges, either K or L, of all magnetic atoms are well located on the hard x-ray spectrum available from synchrotron sources. The resonant enhancement is certainly lower at the K edge, but our experience shows that the difference signals, I^+-I^-, are well measurable from our Fe/Gd multilayer in specular reflection at the Fe K edge. The major part of this signal is the resonant scattering since the nonresonant magnetic scattering approximately scales with $|\mathbf{q}|$, which is very small in multilayer diffraction.

APPENDIX: RECURSION FORMULA FOR MAGNETIC SPECULAR REFLECTIONS

In Parratt's recursion formula[27] for nonmagnetic specular reflections from a multilayer, the complex amplitudes of the electric fields of the transmitted and reflected x-rays in layer j, T_j and R_j, are related to those in layer $j+1$ by

$$\begin{bmatrix} T_j \\ R_j \end{bmatrix} = \widetilde{S}_{j,j+1} \begin{bmatrix} T_{j+1} \\ R_{j+1} \end{bmatrix}, \tag{A1}$$

where $\widetilde{S}_{j,j+1}$ is a 2×2 scattering matrix including δ_m and β_m ($m=j, j+1$), which define the refractive index by $n_j = 1-\delta_j+i\beta_j$ for layer j. T_j and R_j are related by the Fresnel formulas, which are functions of the glancing incidence angle of x-rays on the multilayer surface θ_1. Equation (A1) applies to the plane polarization components of x-rays. In extending this to magnetic scattering, we note that the refractive index of a magnetic medium depends on x-ray circular polarization $n^2=\epsilon\pm iq$. Here ϵ and q are the elements of dielectric tensor $\widetilde{\epsilon}$ of an isotropic medium for an x-ray beam propagating along the magnetization direction:

$$\widetilde{\epsilon} = \begin{bmatrix} \varepsilon & q & 0 \\ -q & \varepsilon & 0 \\ 0 & 0 & \varepsilon \end{bmatrix}.$$

For our experimental geometry shown in Fig. 13, we have

$$\hat{\varepsilon} = \begin{bmatrix} \varepsilon & 0 & -q\cos\psi \\ 0 & \varepsilon & q\sin\psi \\ q\cos\psi & -q\sin\psi & \varepsilon \end{bmatrix}, \tag{A2}$$

where ψ is the angle between the in-plane magnetization $\mathbf{M}$ and the y axis. In Fig. 13, the y-z plane is parallel to the plane of x-ray scattering, defined by the incident and scattered wave vectors $\mathbf{k}$ and $\mathbf{k}'$, and the $+z$ axis is parallel to the outward normal of the multilayer surface. In specular reflection, $\mathbf{k}$ and $\mathbf{k}'$ make angles $-\theta$ and θ to the $+y$ axis respec-
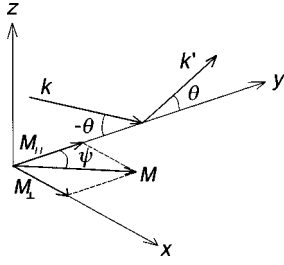
FIG. 13. X-ray specular reflection on a magnetic medium. **M** indicates the in-plane magnetization vector. The x-y plane is parallel to the sample surface and the z axis is defined along the outward normal of the surface. X rays are incident and scattered in the y-z plane. θ is defined to be positive when the z component of a wave vector is positive.

tively, which is along $\mathbf{k}+\mathbf{k}'$. The squared refractive index n^2 derived from Eq. (A2) includes the q^2 and higher terms. When these are neglected against the q term, n is given by

$$n^2 = \varepsilon \pm iq \cos\theta \cos\psi. \tag{A3}$$

The circular polarized light is expressed by

$$E_y = \frac{\pm i\varepsilon \sin\theta\cos\theta - q\sin\theta\cos\psi \pm iq\sin\psi}{\varepsilon\cos\theta} E_x, \tag{A4a}$$

$$H_x = \pm ikn^{\pm}\cos^2\theta \cdot E_x/\mu_0\psi, \tag{A4b}$$

$$H_y = -kn^{\pm}\sin\theta \cdot E_x/\mu_0\psi, \tag{A4c}$$

where the upper and lower signs correspond to the right and left circular polarizations, respectively. Equation (A4a) does not include the approximation of small θ, although the q^2 and higher terms were neglected. We are only interested in the x and y components. We make it clear that right-handed circular light has $+$helicity and left-handed light has $-$ helicity.[28] Any x-ray wave can be expressed as a sum of the right and left circular components. We write $n^+ = 1 - \delta^+ + i\beta^+$ and $n^- = 1 - \delta^- + i\beta^-$ for the refractive indices for right-handed and left-handed circular beams, respectively. Assuming right and left components for each of rays A and B in layer j of a multilayer (Fig. 14), we write for transmitted ray A

$$E_x^A = T_j^+ + T_j^-, \tag{A5a}$$

$$E_y^A = (-a_j\theta_j^+ + b_j)T_j^+ + (-c_j\theta_j^- - b_j)T_j^-, \tag{A5b}$$

$$H_x^A = (ikn_j^+ T_j^+ - ikn_j^- T_j^-)/\mu_0\psi, \tag{A5c}$$

$$H_y^A = (k\theta_j^+ n_j^+ T_j^+ + k\theta_j^- n_j^- T_j^-)/\mu_0\psi, \tag{A5d}$$

and for specular reflected ray B

$$E_x^B = R_j^+ + R_j^-, \tag{A6a}$$

$$E_y^B = (a_j\theta_j^+ + b_j)R_j^+ + (c_j\theta_j^- - b_j)R_j^-, \tag{A6b}$$

$$H_x^B = (ikn_j^+ R_j^+ - ikn_j^- R_j^-)/\mu_0\psi, \tag{A6c}$$

$$H_y^B = (-k\theta_j^+ n_j^+ R_j^+ - k\theta_j^- n_j^- R_j^-)/\mu_0\psi, \tag{A6d}$$
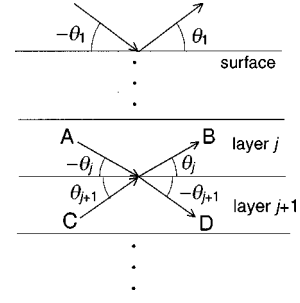
FIG. 14. Specular reflection of x rays in a magnetic multilayer.

where

$$a_j = (i\varepsilon_j - q_j\cos\psi_j)/\varepsilon_j, \tag{A7a}$$

$$b_j = iq_j\sin\psi_j/\varepsilon_j, \tag{A7b}$$

$$c_j = (-i\varepsilon_j - q_j\cos\psi_j)/\varepsilon_j, \tag{A7c}$$

$k = 2\pi/\lambda$ and we assumed a small θ_j. The refraction angles θ_j^+ and θ_j^- are given by Snell's law $n_{j+1}^{\pm}\cos\theta_{j+1}^{\pm} = n_j^{\pm}\cos\theta_j^{\pm}$, where $n_1^{\pm} = 1$ for air above the top surface. Similar expressions hold for the transmitted and reflected rays C and D in layer $j+1$. The continuity of the tangential components of the electric and magnetic fields at the layer interface requires

$$E_x^A + E_x^B = E_x^C + E_x^D, \tag{A8a}$$

$$E_y^A + E_y^B = E_y^C + E_y^D, \tag{A8b}$$

$$H_x^A + H_x^B = H_x^C + H_x^D, \tag{A8c}$$

$$H_y^A + H_y^B = H_y^C + H_y^D. \tag{A8d}$$

A substitution of Eqs. (A5) and (A6), together with those for rays C and D, in Eq. (A8) leads to

$$\begin{bmatrix} T_j^+ \\ T_j^- \\ R_j^+ \\ R_j^- \end{bmatrix} = \tilde{C}_{j,j+1} \begin{bmatrix} T_{j+1}^+ \\ T_{j+1}^- \\ R_{j+1}^+ \\ R_{j+1}^- \end{bmatrix}, \tag{A9}$$

where $\tilde{C}_{j,j+1}$ is a 4×4 scattering matrix. The recursion formula (A9) is reduced to

$$\begin{bmatrix} T_1^+ \\ T_1^- \\ R_1^+ \\ R_1^- \end{bmatrix} = \tilde{C}_{1,2}\tilde{C}_{2,3}\cdots\tilde{C}_{N-1,N} \begin{bmatrix} T_N^+ \\ T_N^- \\ R_N^+ \\ R_N^- \end{bmatrix}, \tag{A10}$$

where N is the number of the layers. One can solve Eq. (A10) by assuming that $R_N^+ = 0$ and $R_N^- = 0$ for an infinitely thick substrate.[27] For a right circular polarized beam incident on the multilayer surface, $T_1^+ = 1$ and $T_1^- = 0$, for example, the specular reflectivity r on the top surface is given by

$$r = |R_1^+|^2 + |R_1^-|^2. \tag{A11}$$

In general, the nondiagonal elements of matrix $\tilde{C}_{j,j+1}$ have nonzero values. Hence the specular reflection is no longer of

pure right circular polarization but includes a left circular component, i.e., $R_1^- \neq 0$ in Eq. (A11). x-ray circular polarizations are mixed by finite-angle scattering on a magnetic medium.

We define the scattering factor of a magnetic atom by[11]

$$f = (\hat{\mathbf{e}}'^*_{\nu'} \cdot \hat{\mathbf{e}}_\nu)(f_0 + f'_c + if''_c) + i(\hat{\mathbf{e}}'^*_{\nu'} \times \hat{\mathbf{e}}_\nu) \cdot \hat{\mathbf{z}}(f'_m + if''_m) \tag{A12}$$

in the dipole approximation, where $f_0 = 64$ for Gd (Thomson scattering), $f'_c (<0)$ and $f''_c (>0)$ are the anomalous dispersion corrections, f'_m and f''_m are the resonant magnetic scattering factors. Unit vector $\hat{\mathbf{z}}$ is along the quantization axis parallel to the local magnetic moment. $\hat{\mathbf{e}}_\nu$ and $\hat{\mathbf{e}}'_{\nu'}$, are the unit polarization vectors of the incident and scattered x-rays, respectively, with ν and ν' indicating the polarization states of the relevant beams. The magnetic scattering factors are given by[11]

$$f'_m + if''_m = -(3/4kr_e)(F_{11} - F_{1-1}), \tag{A13}$$

where F_{LM} is the matrix element of the dipole transition, Gd $2p_{3/2} \rightarrow 5d$ in our case, and r_e is the electron classical radius. Note that Eq. (A12) does not include the $(\hat{\mathbf{e}}'^*_{\nu'} \cdot \hat{\mathbf{z}})(\hat{\mathbf{e}}_\nu \cdot \hat{\mathbf{z}})$ term and the nonresonant magnetic scattering, which are negligible against the $(\hat{\mathbf{e}}'^*_{\nu'} \times \hat{\mathbf{e}}_\nu) \cdot \hat{\mathbf{z}}$ term. The first and second terms of Eq. (A12) represent the charge and resonant magnetic scattering, respectively. We define the charge structure factor F_c and the resonant magnetic structure factor $\mathbf{F}_m$ for a multilayer by

$$F_c = \sum_{\text{all}} {}_j(f_{0j} + f'_{cj} + if''_{cj})\exp(i\mathbf{q} \cdot \mathbf{r}_j), \tag{A14a}$$

$$\mathbf{F}_m = \sum_{\text{mag}} {}_j\hat{\mathbf{z}}_j(f'_{mj} + if''_{mj})\exp(i\mathbf{q} \cdot \mathbf{r}_j), \tag{A14b}$$

giving the total structure factor

$$\mathbf{F}^{\nu'\nu} = (\hat{\mathbf{e}}'^*_{\nu'} \cdot \hat{\mathbf{e}}_\nu)F_c + i(\hat{\mathbf{e}}'^*_{\nu'} \times \hat{\mathbf{e}}_\nu) \cdot \mathbf{F}_m. \tag{A14c}$$

The summation runs over all atoms in Eq. (A14a) and over the resonating magnetic atoms in Eq. (A14b). When squared for intensities, Eq. (A14c) produces cross terms, which are the resonant magnetic-charge interference scattering. The difference intensity measured by flipping the helicity of the incident beam, but not analyzing the polarization of the scattered beam, is given by

$$\sum_{\nu'} |\mathbf{F}^{\nu'+}|^2 - \sum_{\nu'} |\mathbf{F}^{\nu'-}|^2 = -2(\hat{\mathbf{k}} + \hat{\mathbf{k}}' \cos 2\theta) \cdot (F'_c \mathbf{F}'_m$$
$$+ F'_c \mathbf{F}''_m), \tag{A15}$$

where F_c and $\mathbf{F}_m$ are written as sums of the real and imaginary parts:

$$F_c = F'_c + iF''_c, \tag{A16a}$$

$$\mathbf{F}_m = \mathbf{F}'_m + i\mathbf{F}''_m. \tag{A16b}$$

F'_c, F''_c, $\mathbf{F}'_m$, and $\mathbf{F}''_m$ are real quantities for centrosymmetric structures. Equation (A15) shows that the magnetic-charge interference scattering is only sensitive to the magnetization component parallel to $\hat{\mathbf{k}} + \hat{\mathbf{k}}' \cos 2\theta$, which is contained in the plane of scattering.[19,29]

The refractive index parameters are related to f for the forward scattering by

$$\delta = (2\pi n_0 r_e/k^2)\text{Re}\, f(\hat{\mathbf{k}}' = \hat{\mathbf{k}}, \hat{\mathbf{e}}'_{\nu'} = \hat{\mathbf{e}}_\nu), \tag{A17a}$$

$$\beta = (2\pi n_0 r_e/k^2)\text{Im}\, f(\hat{\mathbf{k}}' = \hat{\mathbf{k}}, \hat{\mathbf{e}}'_{\nu'} = \hat{\mathbf{e}}_\nu), \tag{A17b}$$

where n_0 is the atom number per unit volume. For circular polarized beams

$$\delta^{\pm} = (2\pi n_0 r_e/k^2)(f_0 + f'_c \mp f'_m \cos\theta\cos\psi), \tag{A18a}$$

$$\beta^{\pm} = (2\pi n_0 r_e/k^2)(f''_c \mp f''_m \cos\theta\cos\psi). \tag{A18b}$$

At the Gd L_3 edge, the quadrupole component occupies 10% of the total resonant magnetic scattering,[30,31] which we ignored in Sec. III of this paper where we discussed the magnetic structure of the Fe/Gd multilayer.

The resonant scattering factors f'_m and f''_m depend on the local magnetization. When a layer magnetizes nonuniformly along the out-of-plane direction, we divide the layer into p sublayers of uniform magnetization

$$\hat{\mathbf{z}}_j(f'_{mj} + if''_{mj}) \rightarrow \hat{\mathbf{z}}_p S_p(g'_m + ig'_m), \tag{A19}$$

where unit vector $\hat{\mathbf{z}}_p$ and S_p are parameters representing the direction and relative strength of the magnetization of sublayer p, respectively. g'_m and g''_m are the reference resonant magnetic scattering factors, which are common to all sublayers. g'_m and g''_m are energy dependent, whereas $\hat{\mathbf{z}}_p$ and S_p describe the energy-independent sample structure. Correspondingly, we replace f'_m and f''_m in Eq. (A18) by $S_p g'_m$ and $S_p g''_m$, respectively, for the refractive index parameters of nonuniformly magnetized layers.

---

*Present address: Japan Atomic Energy Research Institute, Mikazuki-cho, Hyogo 679-5148, Japan.

†Author to whom correspondence should be addressed. Also at Materials Science Education and Research Center, Nara Institute of Technology, Takayama-cho, Ikoma 630-0101, Japan.

‡Also at Department of Physics and Astronomy, Northwestern University, Evanston, IL 60208.

[1] R. E. Camley, Phys. Rev. B **35**, 3608 (1987).

[2] R. E. Camley and D. R. Tilley, Phys. Rev. B **37**, 3413 (1988).

[3] J. Lepage and R. E. Camley, Phys. Rev. Lett. **65**, 1152 (1990).

[4] Ph. Bauer, M. Sajieddine, C. Dufour, K. Cherifi, G. Marchal, and Ph. Mangin, Europhys. Lett. **16**, 307 (1991).

[5] C. Duford, K. Cherifi, G. Marchal, Ph. Mangin, and M. Hennion, Phys. Rev. B **47**, 14 572 (1993).

[6] M. Sajieddine, Ph. Bauer, K. Cherifi, C. Dufour , G. Marchal, and R. E. Camley, Phys. Rev. B **49**, 8815 (1994).

[7] W. Hahn, M. Loewenhaupt, Y. Y. Huang, G. P. Felcher, and S. S. Parkin, Phys. Rev. B **52**, 16 041 (1995).

[8] H. Hashizume, N. Ishimatsu, O. Sakata, T. Iizuka, N. Hosoito, K. Namikawa, T. Iwazumi, G. Srajer, C. T. Venkataraman, J. C. Lang, C. S. Nelson, and L. E. Berman, Physica B **248**, 133 (1998).

[9] K. Namikawa, M. Ando, T. Nakajima, and H. Kawata, J. Phys. Soc. Jpn. **54**, 4099 (1985).

[10] D. Gibbs, D. R. Harshman, E. D. Isaac, D. B. McWhan, D. Mills, and C. Vettier, Phys. Rev. Lett. **61**, 1241 (1988).

[11] J. P. Hannon, G. T. Grammel, M. Bulme, and D. Gibbs, Phys. Rev. Lett. **61**, 1245 (1988).

[12] S. Ferrer, P. Fajardo, F. de Bergevin, J. Alvarez, X. Torrelles, H. A. van der Vegt, and V. H. Etgens, Phys. Rev. Lett. **77**, 747 (1996).

[13] G. M. Watson, D. Gibbs, G. H. Lander, B. D. Gaulin, L. E. Berman, Hj. Matzke, and W. Ellis, Phys. Rev. Lett. **77**, 751 (1996).

[14] C. Kao, J. B. Hastings, E. D. Johnson, D. P. Siddons, G. C. Smith, and G. A. Prinz, Phys. Rev. Lett. **65**, 373 (1990).

[15] F. de Bergevin, M. Brunnel, R. M. Galéla, C. Vettier, E. Elkaim, M. Bessière, and S. Lefèvre, Phys. Rev. B **46**, 10 772 (1992).

[16] C. C. Kao, C. T. Chen, E. D. Johnson, J. B. Hastings, H. J. Lin, G. H. Ho, G. Meigs, J. M. Brot, S. L. Hulbert, Y. U. Idzerda, and C. Vettier, Phys. Rev. B **50**, 9599 (1994).

[17] J. M. Tonnerre, L. Sève, D. Raoux, G. Soullié, B. Rodmacq, and P. Wolfers, Phys. Rev. Lett. **75**, 740 (1995).

[18] J. F. MaCkay, C. Teichert, D. E. Savage, and M. G. Lagally, Phys. Rev. Lett. **77**, 3925 (1996).

[19] H. Hashizume, N. Ishimatsu, O. Sakata, N. Hosoito, T. Emoto, K. B. Lee, D. R. Lee, and T. Iwazumi, Jpn. J. Appl. Phys. **36**, 4525 (1997).

[20] D. R. Lee, Y. J. Park, S. H. Park, Y. H. Jeong, K. B. Lee, N. Ishimatsu, H. Hashizume, and N. Hosoito, Physica B **248**, 146 (1998).

[21] J. W. Freeland, V. Chakarian, K. Bussmann, Y. U. Idzerda, H. Wende, and C. C. Kao, J. Appl. Phys. **83**, 6290 (1998).

[22] S. W. Lovesey and S. P. Collins, *X-ray Scattering and Absorption by Magnetic Materials* (Oxford Science Publication, Oxford, 1996).

[23] N. Ishimatsu, C. T. Venkataraman, H. Hashizume, N. Hosoito, K. Namikawa, and T. Iwazumi, J. Synchrotron Radiat. **4**, 175 (1997).

[24] D. T. Cromer and D. Liberman, J. Chem. Phys. **53**, 1891 (1970).

[25] F. Baudelet, C. Giorgetti, S. Pizzini, Ch. Brouder, E. Dartyge, A. Fontaine, J. P. Kappler, and G. Krill, J. Electron Spectrosc. Relat. Phenom. **62**, 153 (1993).

[26] C. S. Nelson, G. Srajer, J. C. Lang, C. T. Venkataraman, S. K. Sinha, H. Hashizume, N. Ishimatsu, and N. Hosoito, Phys. Rev. B (to be published 1 November 1999).

[27] L. G. Parratt, Phys. Rev. **95**, 359 (1954).

[28] The handedness of circular polarized light depends on whether the observer is located at the source or downstream. Our definition of the handedness is opposite to the one used by spectroscopists.

[29] This applies to general magnetic scattering. For the perpendicular magnetization, the refractive index is given by $n^2 = \varepsilon + q^2/\varepsilon$, which is very close to $n^2 = \varepsilon$ independent of x-ray polarization.

[30] K. Namikawa (unpublished).

[31] P. Carra, B. N. Harmon, B. T. Thole, A. Altarelli, and G. A. Sawayzky, Phys. Rev. Lett. **66**, 2495 (1991).